High-density Au nanorod optical field-emitter arrays

R G Hobbs[1], Y Yang[1], P D Keathley[1], M E Swanwick[2], L F Velásquez-Garcíia[2], F X Kärtner[1,3], W S Graves[4], and K K Berggren[1*]
[1]Research Laboratory of Electronics, Massachusetts Institute of Technology, Cambridge, MA, U.S.A.
[2]Microsystems Technology Laboratories, Massachusetts Institute of Technology, Cambridge, MA, U.S.A.
[3]Center for Free-Electron Laser Science, Deutsches Elektronen-Synchrotron, Hamburg, Germany
[4]Nuclear Reactor Laboratory, Massachusetts Institute of Technology, Cambridge, MA, U.S.A.

[*]E-mail: berggren@mit.edu

Abstract. We demonstrate the design, fabrication, characterization, and operation of high-density arrays of Au nanorod electron emitters, fabricated by high-resolution electron beam lithography, and excited by ultrafast femtosecond near-infrared radiation. Electron emission characteristic of multiphoton absorption has been observed at low laser fluence, as indicated by the power-law scaling of emission current with applied optical power. The onset of space-charge-limited current and strong optical field emission has been investigated so as to determine the mechanism of electron emission at high incident laser fluence. Laser-induced structural damage has been observed at applied optical fields above 5 GVm^{-1}, and energy spectra of emitted electrons have been measured using an electron time-of-flight spectrometer.

Introduction

Advanced nanofabrication techniques are opening up routes toward improved performance and understanding of electron sources for free-electron lasers [1,2]; optically actuated, ultrafast, temporal electron microscopy and spectroscopy [3–5]; and inverse-Compton scattering x-ray sources [6]. High-resolution electron-beam lithography may facilitate production of bright, ultrafast, high-repetition-rate electron sources via creation of nanoscale electron-emitter dimensions, thus limiting the effective source size, and allowing for improved cathode brightness, and enhancement of the optical field to allow operation at lower applied laser intensity [1,2,6,7]. Additionally, the design of nanostructured metallic photocathodes with localized surface plasmon resonance (LSPR) modes may allow further enhancement of local electric fields, thus allowing increased electron emission via multiphoton absorption or strong optical field emission [1,2,7–12].

Isolated strong optical field emitters may not provide sufficient emission current for applications in ultrafast temporal microscopy and FELs, consequently it is important to understand the limitations of electron emission from nanostructured emitter arrays. For example, dense charge packets produced by pulsed photocathodes can be distorted due to intrinsic space-charge fields present in the packet, resulting in reduced emitter brightness [13]. Distortion of the electron beam and reduced beam brightness may be avoided through careful control of the initial electron distribution at the cathode, or by operating below the threshold for space-charge effects. The study of electron emission dynamics within dense arrays is therefore of fundamental interest for ultrafast, high-brightness photocathode development.

Recently, a number of groups have demonstrated strong optical field emission from both isolated metallic tips, and arrays of tips with nanometer scale tip dimensions [8,10,11,14]. One such report by Bormann *et al.* found that the charge yield produced by optically actuated electron emission from a single Au tip scaled with the 5th power of the incident laser pulse energy at lower laser fluence, which is consistent with a 5-photon absorption process [8]. At higher laser fluence Bormann and co-workers observed a transition of the charge yield dependence on laser intensity from a 5th power relation, to a linear dependence, which is consistent with strong optical field emission. Bormann *et al.* also observed an increase in source brightness at this transition point, which is again supportive of a field-emission mechanism. A recent report by Nagel *et al.* [15], which outlined electron emission from Au nanorod arrays, with larger nanorod dimensions and lower array densities than those investigated in our work, found the charge yield scaled with the square of the laser pulse-energy. Nagel *et al.* interpreted the 2nd order power relationship as being indicative of a strong optical field emission process. In the same work the authors estimated a Keldysh parameter (γ) of 18 for photoemission from a planar Au surface, where $\gamma > 1$ indicates a multiphoton emission process, and thus suggested that the Au pillars enhance the optical field by over 18-fold [11,16]. However, the work of Nagel *et al.* does not consider space-charge at the cathode surface, which may retard electron emission resulting in a lower than expected scaling of charge yield with increasing optical pulse energy. As such, a study of optically actuated electron emission from high-density arrays of nanostructures that accounts for space-charge limited current, strong field effects, and laser induced damage is required.

In this work, we have investigated the characteristics of optically actuated electron emission from high-density arrays of Au nanorods fabricated by electron-beam lithography, and actuated by 35 fs pulses of 800 nm wavelength light from a Ti:Sapphire laser. We have investigated electron emission from Au nanorod emitter arrays with pitches as low as 50 nm and have identified space-charge effects on charge yield, the transition from the multiphoton emission to the strong optical field emission regime, and the onset of laser-induced structural damage to the nanostructured emitters.

Here, we have chosen to investigate Au nanorod arrays as the photocathode material for a number of reasons. High-resolution electron-beam lithography facilitates preparation of Au nanorods in high-density arrays, which are of interest for application in a coherent x-ray generation system based on inverse-Compton scattering, as proposed by Graves *et al.* [6]. Furthermore, Au nanorods exhibit geometry-dependent longitudinal surface-plasmon resonance modes in the near-infrared, which may be tuned to match the driving laser frequency and allow for additional enhancement of the applied optical field at the nanorod apices. We have simulated the enhancement of the optical near-field at Au nanorod surfaces and predicted a field-enhancement factor of ~10 (figure S1). Metallic photocathodes are also desirable due to their relative insensitivity to contamination when compared to high quantum efficiency materials such as alkali halides, and their fast response time. The relative insensitivity of metal photocathodes to contamination allows them to operate under poorer vacuum conditions than alkali halides, thus reducing demands on the photocathode vacuum system.

In this work, Au nanorods were fabricated using electron-beam lithography (EBL) as shown schematically in figure 1 (a). The nanorod arrays were typically fabricated in $7.5\text{-}30 \times 10^3$ μm^2 fields on 15 mm × 15 mm n-Si (1-10 Ω-cm) dies with a 10 nm thick, thermally grown (900 °C, dry O_2) surface layer of SiO_2, which was used to suppress electron emission from the n-Si substrate (675 μm thickness). 100 nm of ZEP-520A (ZEON Corp.) was spin cast at 5 krpm on the Si substrates, baked at 180°C for 2 min, and patterned with a 1 nA beam of 125 keV electrons in an Elionix F-125 EBL system producing single-pixel point exposures at the desired emitter pitch and layout. Typical exposure doses were 5 fC/dot (~3×10^4 electron/dot), for a square array of 10 nm diameter, 100 nm pitch, nanorod emitters. Dot exposures were preferred to area exposures to reduce overall exposure time and thus reduce placement errors within the arrays associated with drift of the electron beam during longer exposures. Exposed ZEP resist was developed by immersion in o-xylene at 0°C for 30 s with constant agitation using a magnetic stirring bar. The sample was then immediately dried under flowing N_2 gas. The EBL resist pattern was then transferred to the underlying 10 nm thick SiO_2 layer using a 40 s CF_4 (10 mTorr, 75 W) reactive-ion-etch (RIE). Ti and Au were evaporated to thicknesses of 3 nm and 45 nm respectively, via electron-beam assisted evaporation ($\leq$0.5 Ås^{-1}, ~10^{-6} mbar) to produce Au nanorods with a Ti adhesion layer. The maximum metal thickness was limited to ~50 nm by the small lateral feature sizes created in the patterned resist (< 15 nm). As the evaporated metal thickness increases it pinches off or closes the opening of the patterned feature in the resist, preventing further deposition of material onto the substrate surface as illustrated in figure 1 (a). The ZEP resist and overlying Ti/Au film were then lifted off in n-methylpyrrolidone at 60 °C, and the sample rinsed with acetone and isopropyl alcohol and dried under a stream of dry N_2 gas. Resist and solvent residues were removed prior to electron emission testing via mild isotropic O_2 plasma cleaning (50 W, 60 s).

SEM images of the Au nanorod arrays were acquired using an FEI Helios Dual Beam SEM-FIB equipped with a high-resolution magnetic immersion lens allowing a resolution of < 1 nm at a working distance of 4 mm at the electron energies used for analysis in this work (typically 5 or 10 keV). Electron emission from Au nanorod arrays was actuated optically using a pulsed Ti:Sapphire amplifier (pulse duration 35 fs, wavelength 800 nm, spectral bandwidth 38 nm, linear polarization, repetition rate 3 kHz). The pulsed light source was focused to a spot (FWHM 90 μm) at the surface of the nanostructured cathode, which was mounted at an angle of 6° with respect to the direction of propagation of the laser pulse within a high-vacuum chamber (~10^{-8} mbar). A schematic of the experimental setup used for electron emission testing is found in figure S2 in the supporting information. A static DC field was applied to the nanostructured cathode via an anode plate 3 mm from the cathode surface. The anode was biased using a Keithley 237 source measurement unit (SMU) capable of applying anode voltages up to 1.1 kV, thus allowing application of a static DC field of up to ~ 0.3 MVm^{-1}. Emission current was measured at both the cathode (Keithley 6485 picoammeter) and the anode (Keithley 237 SMU). Laser power was measured by using a thermal power sensor (Thor Labs S322C). Linear polarization angle was controlled via a half-wave plate upstream of the focusing optics as shown in figure S2.

Results & Discussions

In this work we have investigated the charge yield from Au nanorod array photocathodes as a function of incident laser intensity, laser polarization, nanorod array density, and anode bias, in order to better understand the factors, contributing to, and equally, suppressing, charge production from such photocathodes.

Figure 1 displays a schematic of the fabrication process used to generate the Au nanorod arrays studied in this work, as well as SEM images of the fabricated nanorods. Figure 1 (b) displays the SEM images of arrays of Au nanorods. The larger image displays a top-down SEM image of a 100 nm pitch square array of Au nanorods, while the inset image shows a 45° perspective view of a 50 nm pitch hexagonal array of Au nanorods. The EBL process outlined in the experimental section of this work, allowed fabrication of Au nanorods with 10 nm tip-diameters and 1 nm standard deviation in the tip diameter for 100 nanorods inspected by high-resolution SEM. The Au nanorod height was also found to vary (σ = 5 nm) across a given array as can be seen in the SEM image in the inset of figure 1 (b).

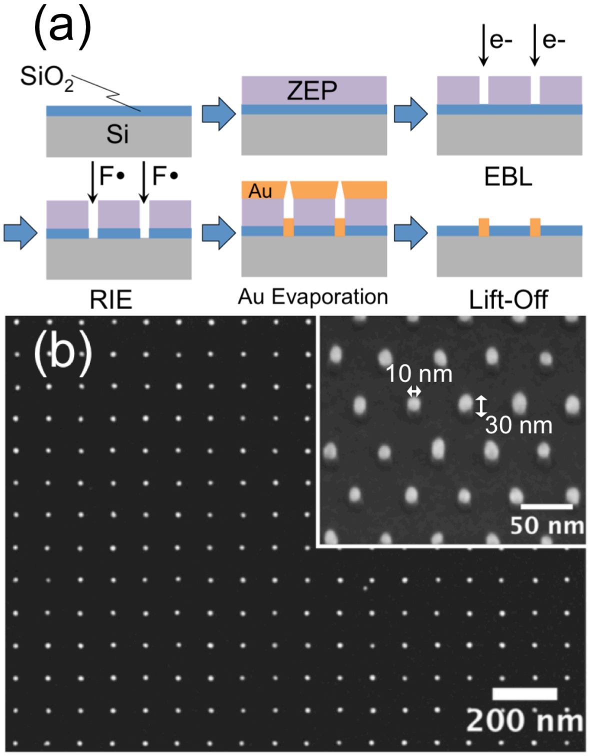

Figure 1. **(a)** Schematic of the Au nanorod array fabrication process. An n-Si wafer with a 10 nm SiO_2 layer was spin-coated with ZEP-520A, patterned by electron-beam lithography using 125 keV electrons, developed and etched by a CF_4 reactive-ion etch to transfer the pattern to the SiO_2 layer. Ti and Au were subsequently evaporated, and lift-off of resist and overlying metal was achieved in a solution of n-methylpyrrolidone. **(b)** Top-down SEM image of a 100 nm pitch square array of Au nanorods. See text for imaging details. Inset, a perspective-view SEM image of a 50 nm pitch hexagonal Au nanorod array, which was acquired at an angle of 45° with respect to the surface of the cathode.

We investigated the mechanism of electron emission from Au nanorods by studying how electron emission current scales as a function of laser intensity, as shown in figure 2 (a), which presents a log-log plot of emission current (I) against incident laser pulse-energy (ε) for a 300 µm × 50 µm area containing a 50-nm-pitch square array of Au nanorods. The current vs. pulse-energy curve displays a distinct kink at ~7 µJ and another less pronounced change in slope above 10 µJ. The fit to the data in figure 2 (a) shows that the relationship between emission current and pulse-energy, below 7 µJ, may be approximated by the expression $I \propto \varepsilon^{4.3}$, which is consistent with a multiphoton absorption process as described by the Fowler-DuBridge model [17]. Here, a 4th- to 5th-order power scaling of emission current with laser pulse energy suggests a cumulative process involving 4- to 5-photon absorption, or equivalently absorption of 6.2-7.75 eV. The observed 5-photon scaling is consistent with previous investigations of electron emission from an isolated Au tip [8]. Au exhibits a high density of filled d-band electronic states ~ 7.0 eV below the vacuum level [18], which is commensurate with the absorption of 4-5 photons of 800 nm light (6.2-7.75 eV). Electron energy spectra (figure S3) of electrons emitted from the Au nanorod arrays display a peak in energy at a relative electron energy of 0.3 eV with a FWHM of 0.5 eV. Consequently, the majority of emitted electrons originate more than 6 eV below the vacuum energy level, and thus well below the Fermi level of Au.

In figure 2 (b), we display the effect of incident linear laser polarization on charge-yield. Emission from Au nanorod arrays was observed to switch off when the linear polarization of the electric field of the laser was rotated from parallel to the long axis of the Au nanorods (p-polarized, black arrow and data in figure 2 (b)) to perpendicular to the nanorods (s-polarized, blue arrow and data in figure 2 (b)). The strong dependence of electron emission on angle of polarization is consistent with the enhancement of the optical field expected at the Au nanorod apex.

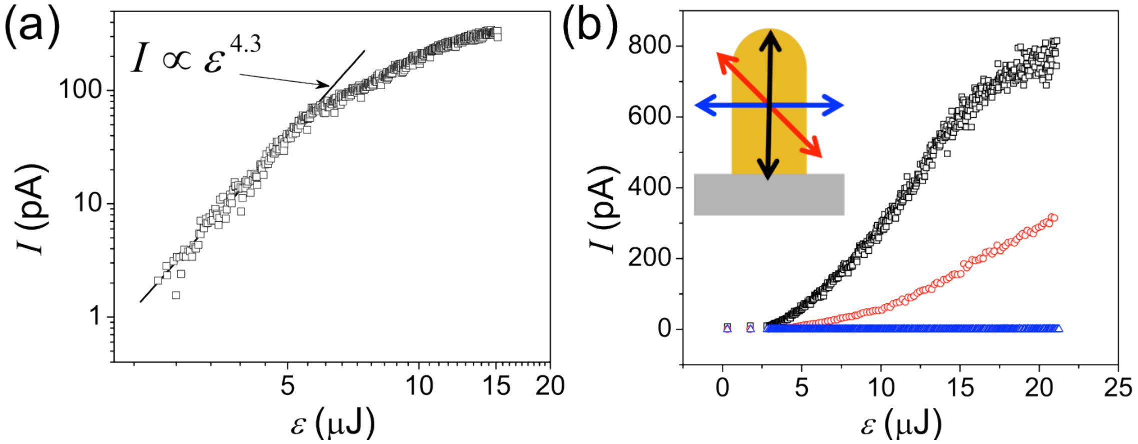

Figure 2. **(a)** Log-log plot of emission current vs. incident laser-pulse energy (ε) for a 300 µm × 50 µm field containing a 50 nm pitch, square array of Au nanorods. Black line represents a 4.3-order power-law scaling of emission current with ε. (b) Polarization dependence of emission current from a 600 µm × 50 µm field containing a 100 nm pitch square array of Au nanorods. The colored arrows indicate the plane of polarization of the electric field in the linearly polarized optical pulses and are color coordinated with emission data in the plot. A gold colored rod is shown schematically to indicate the orientation of the optical field with respect to the geometry of the Au nanorods.

The observed deviation from the n^{th} order power-law scaling at higher pulse energies seen in figure 2 (a), has previously been attributed to the transition from a multiphoton emission regime into a strong optical field emission regime [8,11,15,19]. However, previous reports of emission from Au nanorod arrays have not considered the effects of space-charge on electron-emission from an array of nanoscale emitters. In this work, we have investigated the effects of emitter-array density, and space-charge, on emission behaviour to better understand the underlying mechanism for trends in plots of emission current vs. input optical power. Consequently, we have investigated the charge yield from Au nanorod arrays as a function of array density, the results of which are shown in figure 3.

In Figure 3, we show the relationship between emitter array-density and the point at which emission current deviates from multiphoton emission behavior. Figure 3 shows a normalized log-log plot of electron yield per nanorod tip, per laser pulse (n_{Tip}) vs. pulse-energy, for Au nanorod arrays with varying densities. The emission current from all arrays, irrespective of density, scales with approximately the 5th power of the incident laser pulse-energy at low pulse-energy (< 3 µJ), suggesting a 5-photon absorption mechanism of emission in this pulse-energy range. Figure 3 shows that the value of n_{Tip} at which the charge yield deviates from multiphoton scaling, increases with decreasing array density, which is indicative of space-charge effects. In other words, for arrays with identical n_{Tip} and different array densities, higher density arrays will produce a larger areal charge-density than a lower density array, and thus will present space-charge effects at lower values of of n_{Tip} than lower density arrays. Closer inspection of the raw, unnormalized data presented in the inset of figure 3 reveals that the emission current begins to deviate from behaviour characteristic of multiphoton emission at currents of the order of 10 pA. The dependence of the point of deviation from multiphoton emission behavior, on emission current and not optical intensity, suggests that the deviation is due to the charge-density emitted. Thus, at a specific threshold value of emitted charge from the array, further emission is suppressed. This current suppression due to the density of charge per pulse is known as space-charge-limited current. Space-charge-limited current (I_{SCL}) for pulsed electron emission from a planar surface can be estimated by the single sheet model given by equation (1) [20].

$$I_{\mathrm{SCL}}=\frac{\varepsilon_0 A V f_{\mathrm{laser}}}{d} \tag{1}$$

Here, ε_0 represents vacuum permittivity, A denotes the area of emission (1.5×10^{-8} m^2), V is the anode voltage (100 V), f_{laser} is the repetition rate of the laser (3 kHz) and d is the anode-cathode spacing (3 mm). The single sheet model assumes that distance travelled by the sheet of emitted charge during the duration of the pulse (35 fs) is negligible compared to the total anode-cathode separation. Thus the sheet of emitted charge becomes a virtual cathode and screens the applied static field induced by the anode bias. Screening of the static field prevents emitted electrons from being swept away from the cathode surface and causes an accumulation of charge at the cathode surface, which ultimately prevents further emission from the cathode. The value of I_{SCL} was calculated to be 13 pA for the experimental conditions used to produce the data in figure 3, in the absence of field-enhancement of the applied static field by the Au nanorods. The applied static field may of course be enhanced by the nanostructured emitters. Our simulations (supplementary information) have shown that the static field may be enhanced by a factor of 2-3 in the vicinity of the emitter. Thus I_{SCL} may be 26-39 pA for an anode bias of 100 V. The single sheet model used here may also underestimate the value of I_{SCL} as it does not account for the initial momentum distribution of electrons produced at the cathode surface. The spread in longitudinal and transverse electron momenta may result in electrons escaping the virtual cathode, thus producing higher emission current than predicted by the single sheet model. For example, in the inset of figure 3 we observe emission currents of almost 100 pA despite a maximum estimate of 39 pA for I_{SCL}. Consequently, the cause of the deviation from multiphoton emission behaviour observed in figure 3 is consistent with the onset of the space-charge-limit at the cathode.

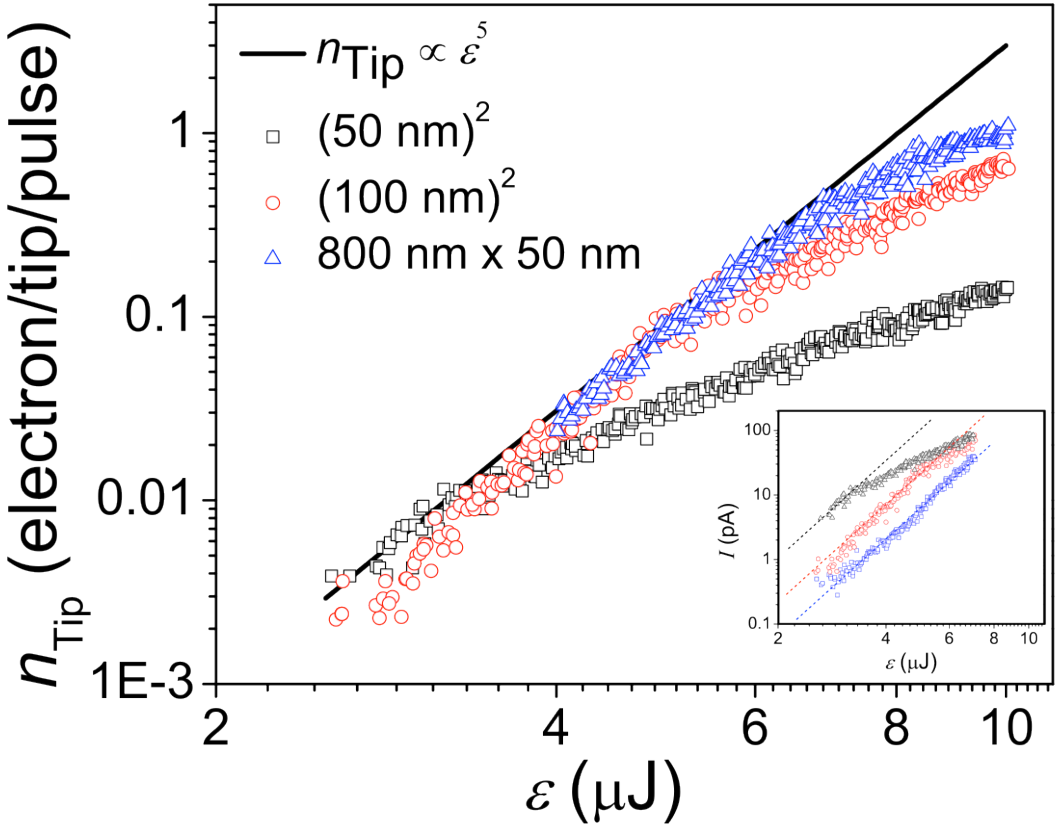

Figure 3. Normalized log-log plot of the average number of electrons emitted per nanorod per pulse vs. incident laser pulse energy (ε) for three arrays of Au nanorods with varied array densities. Black line represents a 5th order power-law scaling of electron yield with pulse energy equivalent to 5-photon absorption. The plot shows that emission from lower density arrays deviates from 5-photon scaling at larger values of pulse energy

than higher density arrays. Inset, a log-log plot of emission current vs. pulse energy, for 300 μm × 50 μm fields of emitters, with various emitter array layouts and an applied anode voltage of 100 V. Black data points represent emission current for a 50-nm-pitch square array of Au nanorods. Likewise, red and blue data points represent a 100-nm-pitch square array, and 800 nm × 50 nm pitch rectangular arrays, respectively. The overlying color-coordinated dashed lines represent 5th order power law curves.

In order to reduce space-charge effects and investigate the underlying emission phenomena, we have investigated emission-current scaling with pulse-energy under higher applied static fields than those used in figure 3. The results of electron emission from a 50-nm-pitch square array of Au nanorods, at anode bias values of 500 V, and 1 kV respectively, are displayed in figure 4 (a). Increasing the applied anode bias should result in an increase in the space-charge-limited current according to equation 1, and thus allow a study of the fundamental scaling of current with laser intensity below this limit. The plot in figure 4 (a) shows a small but distinct kink at 12 pA for both a 500 V and a 1 kV anode bias, which suggests that the kink is not due to space-charge effects, as the emission current at which the kink occurs does not vary significantly with applied anode bias as would be expected from equation 1. This result suggests another underlying mechanism as the cause for the observed kink in the emission curve.

Strong optical field emission of electrons via quantum tunnelling has previously been shown to follow a cycle-averaged Fowler-Nordheim-type behaviour[11]. A linear dependence of $\ln(I/E^2)$ on $1/E$, where E represents the peak applied optical field of the incident laser, and I represents the emission current, is characteristic of strong-field tunnelling within the WKB approximation. Figure 4(b) displays Fowler-Nordheim-type plots for the data above the kink in figure 4(a). The Fowler-Nordheim-type plots in figure 4(b) display linear behavior at lower values of optical-field strength. A linear fit to the datasets in figure 4(b) for values of $1/E > 2.5 \times 10^{-10}$ V^{-1}m, gives a line with a slope (B) of 9.5×10^9 Vm^{-1}. The field-enhancement factor (α) of the nanorod for the optical field can be calculated from the expression, $\alpha = b\phi^{3/2}/B$, where b is a universal constant of value $6.830\,890 \times 10^9$ eV$^{-3/2}$ Vm^{-1}, and ϕ is the work function of Au (~5.3 eV). A value of $\alpha = 9$ has been found for the Au nanorods examined in the present work.

The plots in figure 4 (b) are observed to deviate from linear behaviour at higher values of emission current, which has previously been attributed to the onset of space-charge effects in conventional DC field emitters [21]. For example, the data in figure 4 (b) acquired at an anode bias of 500 V, saturates at a value of $1/E = 2.1 \times 10^{-10}$ V^{-1}m, which is equivalent to an emission current of 125 pA. The space-charge-limited current for an anode bias of 500 V, calculated using equation 1, is 66 pA. The observed discrepancy in the value of I_{SCL} suggests that the applied static field is enhanced by a factor of 1.9 by the nanorod emitters. Results of simulations of the static field enhancement at a Au nanorod surface are shown in figure S4, and confirm that field enhancement in the range of 2 to 10 times can be expected for an isolated Au nanorod. Confirmation that emission from such an array of Au nanorods is space-charge-limited at an incident pulse-energy of 7 μJ, and anode bias of 500 V can be seen in figure S5. Figure S5 shows that the emission current for a 50 nm pitch square array of Au nanorods scales linearly with applied anode bias for a pulse energy of 7 μJ, as expected for space-charge-limited emission.

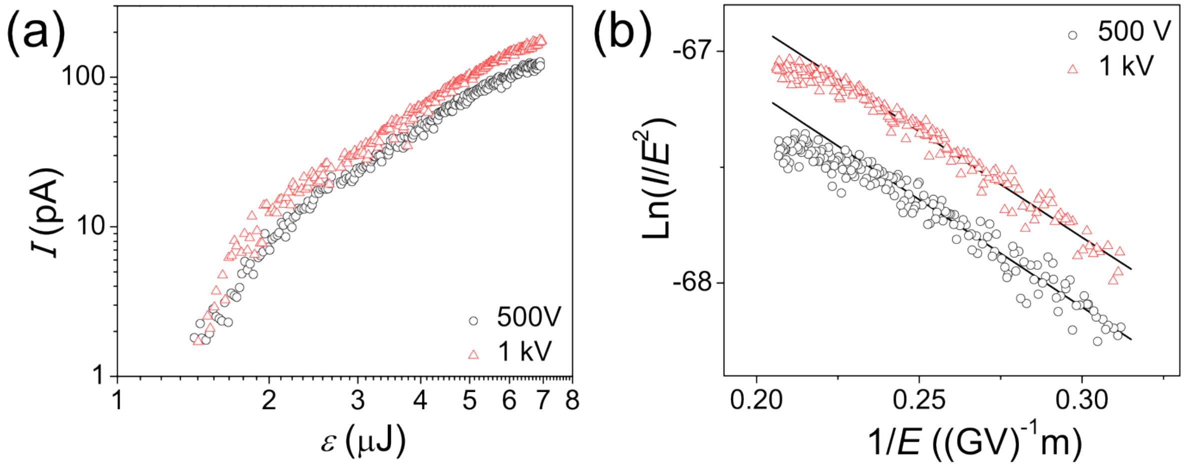

Figure 4. (a) Log-log plot of emission current (*I*) against laser pulse-energy (*ε*) for a 50 nm pitch array of Au nanorod emitters. (b) Fowler-Nordheim plot of electron emission from a 50 nm pitch array of Au nanorods at anode bias values of 500 V and 1 kV. The inverse of the peak optical field (*E*) is plotted against $\ln(I/E^2)$ for values of *I* above the kink point in (a), where *I* represents the average emission current. Solid lines represent linear fits to the data in the low current regime. A field enhancement factor $\alpha = 9$ has been extracted from the slope of the linear fits.

The data presented in figure 4 thus suggests that the emission behaviour of Au nanorod emitter arrays investigated in this work has three regimes, which given in order of increasing laser intensity are, (1) multiphoton absorption, (2) strong optical field emission, and (3) space-charge limited current. Strong optical field emission is expected to occur for systems with a Keldysh parameter of $\gamma < 2$. In this work, emission from Au nanorod arrays has been observed to diverge from multiphoton emission behaviour at incident laser pulse-energy values in the range of 2-6 μJ, or equivalently $4 < \gamma < 7$ in the absence of localized field enhancement. Consequently, the expected field enahncement factor based on this analysis should be in the range 2-4, which is similar to the value of $\alpha = 9$ calculated from figure 4 (b).

Figure 5 shows results of 3-D numerical simulations of the electric field strength in the vicinity of Au nanorod arrays of varying density, which were performed by the finite element method (FEM) using *COMSOL Multiphysics*. Details of the simulation model can be found in the supplementary information. Peak enhancement of the optical field at the apices of the nanorods was found to range from a factor of 4.1 for 50 nm pitch rods, to a factor of 12.7 for a rectangular array with 800 nm pitch in *x* and a 50 nm pitch in *y*. The observed increase in field-enhancement with decreasing array density in the simulation results shown in figure 5 are consistent with an increased effect of charge screening due to proximity effects in denser arrays. In figure 4 (a) we have observed a transition from the multiphoton absorption regime to the strong optical field emission regime at 2 μJ pulse-energy ($\gamma = 7$) for a 50 nm pitch nanorod array. The simulated optical field enhancement factor of 4.1 estimated for a 50 nm pitch array (figure 5 (a)) would thus result in an enhanced Keldysh parameter of $\gamma < 2$. A Keldysh parameter of $\gamma = 2$ has been shown to accurately predict the optical intensity at which a photoemission process transitions from a multiphoton absorption mechanism to a strong field tunneling mechanism [8,22,23]. Consequently, the simulation results presented in figure 5 suggest that the kink in the emission current plots shown in figure 4(a) are likely to be due to the transition from multiphoton emission to tunneling emission.

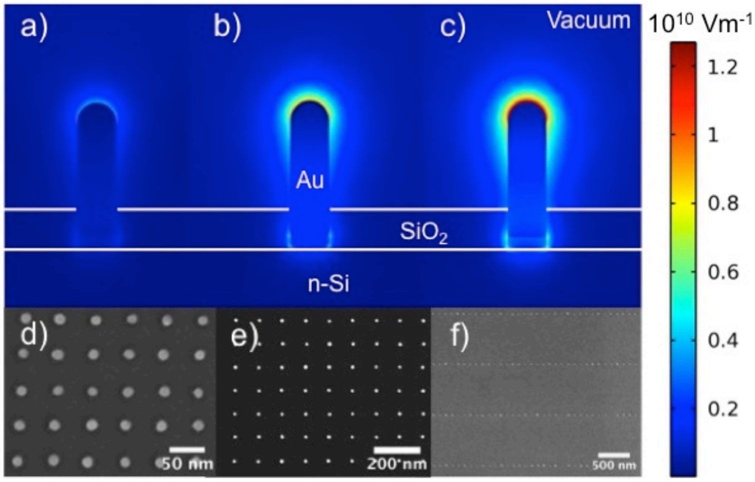

Figure 5. (a-c) Cross-section of electric field strength simulated in the vicinity of Au nanorod arrays with pitches of (a) 50 nm, (b) 100 nm, and (c) 800 nm in *x* and 50 nm in *y*. Peak field enhancement values were simulated to be 4.1, 9.3 and 12.7 for (a), (b) and (c) respectively. (d-f) Top-down SEM images of Au nanorod arrays with pitches corresponding to the simulation results in (a-c).

The effects of laser power on the morphology of the Au nanorods studied in this work was also investigated experimentally (figure S6). Structural changes indicative of field evaporation of Au were observed at high laser fluence. SEM images of these structural changes can be found in the supporting information. Morphological changes were observed in ~10% of Au nanorods illuminated with 18 μJ pulses of 800 nm light, 2% of nanorods illuminated with 15 μJ pulses, and < 0.5 % of nanorods exposed to 10 μJ pulses. Consequently, the incident laser pulse energy was restricted to less than 10 μJ for the majority of emission studies presented in this work. The effect of laser-induced heating in the Au nanorods have also been considered and details of this investigation can be found in the supporting information.

The quantum efficiency (QE) of a photocathode is a key metric in determining its efficiency, and is defined as the number of electrons produced per photon incident upon that photocathode. A QE of ~ 10^{-9} has been calculated for electron emission excited by 800 nm light from 800 nm × 50 nm pitch rectangular Au nanorod arrays fabricated in this work within the 5-photon absorption regime. The value of QE does not account for the dead space between Au nanorods in the array, nor does it account for dead space outside of the array. Thus, an internal quantum efficiency (QE_{int}) can be defined as the number of electrons produced from the Au nanorod array per photon of 800 nm light incident on the Au component of the substrate. QE_{int} has been calculated, in the absence of near-field focusing, as ~ 10^{-7} for the lower-density (800 nm × 50 nm) Au nanorod arrays produced in this work. Of course, as shown in figures 4 and S5, the charge yield from the Au nanorod arrays depends strongly on the applied static field, as such the QE may increase significantly under a higher applied static field, as is easily achieved in a RF-gun. The QE of the IR driven Au nanorod cathode seems low when compared to the QE of a typical planar Au cathode driven by a UV light source ($QE_{Cu} \sim 10^{-4}$). However, when factors such as the efficiency of UV light generation and the difference in energy between an IR and UV photon are considered, the QE of this Au nanorod compares well with that of a typcial metal photocathode driven by a UV light source. A typical conversion efficiency from IR to UV by fourth harmonic generation is 10%, and the photon energy of the UV photon produced is 4 times that of the IR photon used in this experiment. Therefore, a fair comparsion of the Au cathode driven by IR would be to compare 40 times QE_{int} for the Au nanorods in this work *i.e.* $QE_{\text{int}} \sim 10^{-5}$, to QE of a typical metallic UV-driven photocathode *e.g.* $QE_{Cu} = 1.4 \times 10^{-4}$ or $QE_{Nb} = 2 \times 10^{-5}$ [13].

In conclusion, the results presented in this work support a strong optical-field-emission mechanism for electrons produced from high-density arrays of Au nanorods prepared by electron beam lithography and illuminated with 35 fs pulses of 800 nm light with ~1 GVm^{-1} optical fields. The onset of space-charge-limited emission current has been observed at the low applied static fields used in this work. Laser-induced damage to the Au nanorods has been observed at high laser fluence equivalent to optical fields greater than 5 GVm^{-1}. Ultrafast electron emission from high-density nanostructured emitters, via strong optical-field emission opens up opportunities for production of high current-density, ultrafast and bright electron beams. Such emitters will be suitable for applications in temporal electron spectroscopy, diffraction, and microscopy, as well as next-generation x-ray sources.

Acknowledgements
We acknowledge financial support from DARPA under contract N66001-11-1-4192, and the Gordon and Betty Moore Foundation. The authors would like to acknowledge Dr. Tim Savas, Mr. Mark Mondol, and Mr. Jim Daley of the NanoStructures Laboratory at MIT, and Mr. Vitor Manfrinato, and Dr. Lin-Lee Cheong for helpful advice regarding nanorod fabrication.

References

[1] Li R K, To H, Andonian G, Feng J, Polyakov A, Scoby C M, Thompson K, Wan W, Padmore H A and Musumeci P 2013 Surface-Plasmon Resonance-Enhanced Multiphoton Emission of High-Brightness Electron Beams from a Nanostructured Copper Cathode *Phys. Rev. Lett.* **110** 074801

[2] Polyakov A, Senft C, Thompson K F, Feng J, Cabrini S, Schuck P J, Padmore H A, Peppernick S J and Hess W P 2013 Plasmon-Enhanced Photocathode for High Brightness and High Repetition Rate X-Ray Sources *Phys. Rev. Lett.* **110** 076802

[3] Zewail A H 2006 4D ultrafast electron diffraction, crystallography, and microscopy *Annu. Rev. Phys. Chem.* **57** 65

[4] Siwick B J, Dwyer J R, Jordan R E and Miller R J D 2002 Ultrafast electron optics: Propagation dynamics of femtosecond electron packets *J. Appl. Phys.* **92** 1643

[5] Corkum P B and Krausz F 2007 Attosecond science *Nat. Phys.* **3** 381

[6] Graves W S, Kärtner F X, Moncton D E and Piot P 2012 Intense Superradiant X Rays from a Compact Source Using a Nanocathode Array and Emittance Exchange *Phys. Rev. Lett.* **108** 263904

[7] Hommelhoff P, Sortais Y, Aghajani-Talesh A and Kasevich M A 2006 Field Emission Tip as a Nanometer Source of Free Electron Femtosecond Pulses *Phys. Rev. Lett.* **96** 077401

[8] Bormann R, Gulde M, Weismann A, Yalunin S and Ropers C 2010 Tip-Enhanced Strong-Field Photoemission *Phys. Rev. Lett.* **105** 147601

[9] Dombi P, Horl A, Racz P, Marton I, Trugler A, Krenn J R and Hohenester U 2013 Ultrafast Strong-Field Photoemission from Plasmonic Nanoparticles *Nano Lett.* **13** 674

[10] Krüger M, Schenk M and Hommelhoff P 2011 Attosecond control of electrons emitted

from a nanoscale metal tip *Nature* **475** 78

[11] Keathley P D, Sell A, Putnam W P, Guerrera S, Velasquez-Garcia L and Kaertner F X 2012 Strong-field photoemission from silicon field emitter arrays *Ann. Phys. Berlin* **525** 144

[12] Dombi P, Irvine S E, Rácz P, Lenner M, Kroó N, Farkas G, Mitrofanov A, Baltuška A, Fuji T, Krausz F and Elezzabi A Y 2010 Observation of few-cycle, strong-field phenomena in surface plasmon fields *Opt. Express* **18** 24206

[13] Dowell D H, Bazarov I, Dunham B, Harkay K, Hernandez-Garcia C, Legg R, Padmore H, Rao T, Smedley J and Wan W 2010 Cathode R&D for future light sources *Nucl. Instrum. Meth. A* **622** 685

[14] Swanwick M E, Keathley P D, Fallahi A, Krogen P R, Laurent G, Moses J, Kärtner F X and Velásquez-García L F 2014 Nanostructured Ultrafast Silicon-Tip Optical Field-Emitter Arrays. *Nano Lett.* [Online early access]

[15] Nagel P M, Robinson J S, Harteneck B D, Pfeifer T, Abel M J, Prell J S, Neumark D M, Kaindl R A and Leone S R 2013 Surface plasmon assisted electron acceleration in photoemission from gold nanopillars *Chem. Phys.* **414** 106

[16] Keldysh L V. 1965 Ionization in the field of a strong electromagnetic wave *Sov. Phys. JETP* **20** 1307

[17] Bechtel J H, Smith W L and Bloembergen N 1977 Two-photon photoemission from metals induced by picosecond laser pulses *Phys. Rev. B* **15** 4557

[18] Krolikowski W F and Spicer W E 1970 Photoemission Studies of the Noble Metals II Gold *Phys. Rev. B* **1** 478

[19] Krüger M, Schenk M and Hommelhoff P 2011 Attosecond control of electrons emitted from a nanoscale metal tip. *Nature* **475** 78–81

[20] Valfells A, Feldman D W, Virgo M, O'Shea P G and Lau Y Y 2002 Effects of pulse-length and emitter area on virtual cathode formation in electron guns *Phys. Plasmas* **9** 2377

[21] Jensen K L 1999 Field emitter arrays for plasma and microwave source applications *Phys. Plasmas* **6** 2241

[22] Yalunin S V., Gulde M and Ropers C 2011 Strong-field photoemission from surfaces: Theoretical approaches *Phys. Rev. B* **84** 195426

[23] Piglosiewicz B, Schmidt S, Park D J, Vogelsang J, Groß P, Manzoni C, Farinello P, Cerullo G and Lienau C 2013 Carrier-envelope phase effects on the strong-field

photoemission of electrons from metallic nanostructures *Nat. Photonics* **8** 37